



**HAL**  
open science

# Stochastic simulation of reference rainfall scenarios for hydrological applications using a universal multifractal approach

Arun Ramanathan, Pierre-Antoine Versini, Daniel Schertzer, Remi Perrin, Lionel Sindt, Ioulia Tchiguirinskaia

## ► To cite this version:

Arun Ramanathan, Pierre-Antoine Versini, Daniel Schertzer, Remi Perrin, Lionel Sindt, et al.. Stochastic simulation of reference rainfall scenarios for hydrological applications using a universal multifractal approach. *Hydrology and Earth System Sciences*, 2022, 26 (24), pp.6477-6491. 10.5194/hess-2021-580. hal-04144674

**HAL Id: hal-04144674**

**<https://enpc.hal.science/hal-04144674v1>**

Submitted on 28 Jun 2023

**HAL** is a multi-disciplinary open access archive for the deposit and dissemination of scientific research documents, whether they are published or not. The documents may come from teaching and research institutions in France or abroad, or from public or private research centers.

L'archive ouverte pluridisciplinaire **HAL**, est destinée au dépôt et à la diffusion de documents scientifiques de niveau recherche, publiés ou non, émanant des établissements d'enseignement et de recherche français ou étrangers, des laboratoires publics ou privés.



# Stochastic simulation of reference rainfall scenarios for hydrological applications using a universal multifractal approach

Arun Ramanathan<sup>1</sup>, Pierre-Antoine Versini<sup>1</sup>, Daniel Schertzer<sup>1</sup>, Remi Perrin<sup>2</sup>, Lionel Sindt<sup>2</sup>, and Ioulia Tchiguirinskaia<sup>1</sup>

<sup>1</sup>École des Ponts Paristech (ENPC), Laboratory of Hydrology Meteorology & Complexity

<sup>2</sup>SOPREMA

**Correspondence:** Arun Ramanathan (arun.ramanathan@enpc.fr)

**Abstract.** Hydrological applications such as storm-water management or flood design usually deal with and are driven by region-specific reference rainfall regulations or guidelines based on Intensity-Duration-Frequency (IDF) curves. IDF curves are usually obtained via frequency analysis of rainfall data using which the exceedance probability of rain intensity for different durations are determined. It is also rather common for reference rainfall to be expressed in terms of precipitation  $P$ , accumulated in a duration  $D$  (related to rainfall intensity  $\frac{P}{D}$ ), with a return period  $T$  (inverse of exceedance probability). Meteorological modules of hydro-meteorological models used for the aforementioned applications therefore need to be capable of simulating such reference rainfall scenarios. The multifractal cascade framework, since it incorporates physically realistic properties of rainfall processes (non-homogeneity or intermittency, scale invariance and extremal statistics) seems to suit this purpose. Here we propose a discrete-in-scale universal multifractal (UM) cascade based approach. Daily, Hourly and six-minute rainfall time series datasets (with lengths ranging from 100 to 15 years) over three regions (Paris, Nantes, and Aix-en-Provence) in France that are characterized by different climates are analyzed to identify scaling regimes and estimate corresponding UM parameters ( $\alpha, C_1$ ) required by the UM cascade model. Suitable renormalization constants that correspond to the  $P, D, T$  values of reference rainfall are used to simulate an ensemble of reference rainfall scenarios, and the simulations are finally compared with datasets. Although only purely temporal simulations are considered here, this approach could possibly be generalized to higher spatial dimensions as well.

**Keywords.** Multifractals, Non-linear geophysical systems, Cascade dynamics, Scaling, Hydrology, Stochastic rainfall simulations.

## 1 Introduction

Reference rainfall events characterized by amount of precipitation  $P$ , duration  $D$  and return period  $T$  are required for sizing storm-water management infrastructures such as conduits, retention basin, and even green roofs if considered as a storm-water management tool. Uniform rainfall or synthetic hyetograms that do not consider the high spatio-temporal variability of rainfall fields are traditionally used for such purposes (Qiu et al., 2021). Therefore, stochastic simulation of reference rainfall events is necessary. There are several types of stochastic rainfall models as listed below: Simple point processes (Salas, 1993), Cluster



processes (Cowpertwait, 1994; Cameron et al., 2000b, a), Hybrid processes (Gyasi-Agyei and Willgoose, 1999; Onof et al.,  
25 2000), and Hydrogram (temporal distribution of discharge) models such as SHYPRE - Simulation of hydrograms for the pre-  
determination of floods and SHYREG - Regionalized SHYPRE (Arnaud and Lavabre, 1999). While all these models are purely  
temporal, Hydrogram models use the Monte Carlo method to generate hyetograms (temporal distribution of rainfall intensity).  
Markov chain (Wilks, 1998), and Non-parametric (Rajagopalan and Lall, 1999; Brandsma and Buishand, 1998) models, on  
the other hand, simulate rainfall time series at a few distinct spatial points and can therefore be considered to be slightly  
30 more advanced than purely temporal models. Cell clusters (Wheater et al., 2000), Modified turning band (Shah et al., 1996),  
Radar-based bead (Pegram and Clothier, 2001) models can be considered are a bit more involved than the aforementioned  
models, however they do make some non-physical simplifying assumptions and are still not that parsimonious. Alternatively,  
there are other procedures utilizing point models (Cowpertwait et al., 1996), and artificial neural networks (Burian et al., 2001)  
that generally deal with downscaling of rain fields from numerical weather prediction (NWP) models. Finally there are a few  
35 physically-based yet computationally simple and parsimonious models such as Non-homogeneous random cascades (Schertzer  
and Lovejoy, 1988, 1989, 2004a, b) that take into consideration the realistic spatio-temporal complexity of rainfall fields.

To make a literature-based assessment of these modelling approaches we consider six characteristics of observed rainfall  
fields that if incorporated by the framework makes the simulations physically relevant/realistic: 1) Heterogeneity – the statisti-  
cal properties of the field are spatial-location dependant resulting in extreme variability especially at small scales 2) Physically  
40 based – the simulations rely on physical principles, 3) Nonlinearity – for instance, fields are not presumed to be additive, 4)  
Space-time complexity – both spatial and temporal variability/properties of the field can be considered simultaneously thereby  
incorporating possible space-time anisotropy, 5) Extreme statistics – extreme rainfall values are more frequent than usual re-  
sulting into strongly non-Gaussian statistics, 6) Statistical non-stationarity with the possibility of long-term memory – the  
statistical properties of the field being auto-correlated over larger temporal lags. Two additional characteristics that make the  
45 model practically attractive are also considered for the assessment: 7) High Parameter parsimony – the model uses only a few  
parameters, 8) Low Computational complexity – the entire simulation procedure including parameter estimation is not too  
time consuming. The existence of simplifying physical principles such as universality help the frameworks in being highly  
parsimonious and computationally simple without compromising too much on the physical relevance of the simulations. Table.  
1 shows a literature-based comparison of the desirable characteristics possessed by each model sub-classification. As shown in  
50 Fig. 1 most of the aforementioned models (10 out of 12) seem to be more focussed on computational and conceptual simplic-  
ity than on physics. Alternatives such as Universal Multifractal (UM) cascades that aren't computationally that complicated  
(compared to high-resolution Numerical Weather Prediction models that explicitly represent given atmospheric processes on  
a limited range of scale) therefore seem to be attractive choices especially since they are capable of representing fields with  
high spatio-temporal variability (Schertzer and Lovejoy, 1989; Ladoy et al., 1993; Tessier et al., 1996; Lovejoy and Schertzer,  
55 2006, 2007; Schertzer et al., 2010; Schertzer and Lovejoy, 2011; Hoang et al., 2012; Lovejoy and Schertzer, 2013; Gires et al.,  
2013; Hoang et al., 2014).

The objective of this paper is to simulate region specific reference rainfall scenarios which could be used as realistic inputs  
(as they exhibit larger variability and intermittency over a wide range of scales compared to uniform rainfall or synthetic



60  
65  
hyetograms) to hydrological models for optimally designing storm-water management infrastructures. This paper attempts to understand the possibility of simulating reference rainfall ensembles characterized by the required properties (P,D,T) while exhibiting temporal variability and intermittency close to that of observed rainfall data. Section 2 discusses the different regions considered in France, their corresponding reference rainfall regulations and the observational datasets used. These rainfall datasets are analysed via multifractal techniques as shown in Section 3 to identify scaling regimes and corresponding UM parameters necessary to simulate rainfall. Section 4 gives a brief recollection about discrete-in-scale UM cascades, explains in detail the procedure used here to simulate reference rainfall scenarios, and finally defines four metrics to quantitatively compare the simulations with corresponding datasets. Finally, the conclusions of this study along with its limitations and some future scope (extension to higher dimensions and other regions) are discussed in Section 5.

## 2 Regions considered and observational datasets used

70  
75  
80  
85  
French regional storm-water management/discharge regulations are usually expressed in relation with some reference rainfall events expressed in terms of precipitation  $P$ , duration  $D$ , return period  $T$  values. As shown in Table. 2 the  $P,D,T$  values - for 3 different localities - display high variability, but this is not that surprising since these values correspond to reference rainfall and rainfall like many other geophysical fields exhibits high spatio-temporal variability. As seen from the  $P,D,T$  combinations for Nantes and Aix-en-Provence it is very clear that these specifications are highly variable even within the same region considered and the corresponding hydrological designs have to take into account such high space-time variability of rainfall at least up to (and in fact more than) these legal constraints or regulations. Therefore, it is quite logical that the modelling technique to be used for stochastically simulating an ensemble of such highly variable reference rainfall scenarios should explicitly incorporate properties of heterogeneity and Non-Gaussian statistics among several other properties that the observed fields typically exhibit. The rainfall datasets used for the three regions (Paris, Nantes and Aix-en-Provence) were obtained from MeteoFrance. Different time series were collected according to the time step (6-minute, hourly, daily). Figure. 2 shows the selected conurbations and their climatological rainfall data. These three regions were selected for this study as their monthly cumulative rainfall climatology (computed from daily data sets) are quite different from each other: while Paris receives around 40-60 mm monthly rainfall, Nantes receives a higher monthly rainfall from around 40-90 mm, Aix-en-Provence on the other hand receives a more variable monthly rainfall from around 10-80 mm. Cities are chosen here since storm-water management is more vital in urban areas due to their limited infiltration capacity. Information about the datasets used for each city/conurbation are given in Table 3. Since the proportion of data missing is low, replacing these values with zeros will probably not result in any significant change to the actual data. For the sake of simplicity, we shall henceforth refer to the daily, hourly and 6-minutes datasets of Paris, Nantes and Aix as PD1, PD2, PD3, ND1, ND2, ND3, AD1, AD2, AD3 respectively.



### 3 Regions considered and observational datasets used

The concept of universality in complex systems states that only a few parameters (out of many) are relevant for defining the system since the same dynamical process is repeated scale after scale or the process interacts with many independent processes over a range of scales resulting in this reduction (Schertzer and Lovejoy, 1987; SCHERTZER et al., 1991; Schertzer and Lovejoy, 1997). In the UM framework only three parameters  $\alpha, C_1, H$  (therefore referred to as UM parameters) are necessary. The three universal multifractal parameters have different geometrical and physical meanings. The degree of multifractality  $\alpha$  defines the deviation from monofractality and its value is between 0 and 2 (if  $\alpha = 0$  the process is mono-/uni- fractal with a unique fractal scaling exponent contrary to other cases ( $\alpha \neq 0$ ), if  $\alpha = 2$  the process has maximum multifractality with a larger spectrum of scaling exponents), codimension of the mean  $C_1$  which describes the sparseness of the level of activity that dominantly contributes to the mean field ( $C_1 = 0$  if the rainfall is homogeneous or in other words, if it always rains). The parameter  $H$  (not exactly the same as Hurst's exponent but related to it) quantifies the deviation from a conservative process ( $H = 0$ ), where the ensemble average of the field is conserved or in other words the ensemble average of the normalized field is 1. In a stochastic multifractal formalism, the  $q$ -th order statistical moment of rainfall  $R_\lambda$  observed at a scale  $l$  follows the multiscaling equation:

$$\langle R_\lambda^q \rangle = \lambda^{K(q)} \quad (1)$$

where  $\lambda$  is the intermediate scale ratio or resolution (ratio of the largest scale to the intermediate scale  $l$ ), the equality sign is used here in a scaling sense, and the scaling exponent  $K(q)$  is the scaling moment function that is scale-independent. For conservative UM,  $K(q)$  depends only on the UM parameters as follows:

$$K(q) = \begin{cases} \frac{C_1}{\alpha-1}(q^\alpha - q) & \forall \quad 0 \leq \alpha < 1, \quad 1 < \alpha \leq 2 \\ C_1 q \log q & \forall \quad \alpha = 1 \end{cases} \quad (2)$$

By computing the trace moments and double trace moments the function  $K(q)$  and UM parameters can be empirically estimated (Schertzer and Lovejoy, 1987; Lavalée et al., 1993) as briefly discussed in the following two subsections. We consider each observational dataset to be a single sample (to avoid any reduction in the largest scale considered which may lead to different multifractal characteristics). However, there is a drawback due to this small sample size: the estimate of spectral slope  $\beta$  is unreliable (coefficient of determination of the straight line fit is too low). Since  $H = \frac{\beta + K(2) - 1}{2}$ , consequently the  $H$  values estimated using  $\beta$  are also not very accurate. Therefore  $H$  is estimated by considering the first order ( $q = 1$ ) un-normalized trace moment  $\langle R_\lambda^1 \rangle$  (initially) assuming that the field is non-conservative

$$\langle R_\lambda^1 \rangle = \lambda^{-H} \quad (3)$$

where once again equality sign is used for a possible asymptotic equivalence ( $\lambda \rightarrow \infty$ ).

It turns out that for all the datasets (from PD1 to AD3) the slope of a straight line fitted through a log-log plot of  $\langle R_\lambda^1 \rangle$  vs.  $\lambda$  is close to zero, implying  $H \approx 0$  (as shown in Table. 4). Therefore, we proceed by assuming the observed rainfall used in this study are conservative fields.



### 3.1 Trace Moment (TM) Analysis

120 In the TM analysis (Tessier et al., 1993; Schertzer and Lovejoy, 1987, 1992) rainfall  $R_\Lambda$  at the finest given resolution or scale ratio ( $\Lambda = \frac{\text{largest scale}}{\text{smallest scale}}$ ) is averaged to obtain rainfall over coarser and coarser resolutions  $R_\lambda$ , where the intermediate scale ratio  $\lambda$  is a decreasing integer power of  $\lambda_1$  ( $\lambda = \lambda_1^n, \Lambda = \lambda_1^N; n = N, \dots, 0$ ), which is the scale ratio of the elementary cascade step and usually equals 2:

$$R_{\lambda_1^n}(j) = \frac{1}{\lambda_1} \sum_{i=1}^{\lambda_1} R_{\lambda_1^{n+1}}(\lambda_1(j-1) + i); \quad j = 1, 2, \dots, \lambda_1^n; \quad n = N-1, \dots, 0 \quad (4)$$

125 Since rainfall fields are multifractals their statistics follow the multiscaling equation Eq. (1), therefore the trace moments at coarser and coarser resolutions  $TM_\lambda = \frac{\langle R_\lambda^q \rangle}{\langle R_\lambda \rangle^q}$  when plotted vs.  $\lambda$  in a log-log coordinate can be used to estimate the slope  $K(q)$  of a fitted straight line. Figure. 3 shows the results of this analysis done on all the datasets (PD1 to AD3): there are two scaling regimes having distinct slope or  $K(q)$  with a scaling break (the scale where  $K(q)$  changes abruptly and distinctly) at around 2 to 4 weeks. This break in temporal scaling can be attributed to the synoptic maximum (Tessier et al., 1996) or in other  
 130 words the lifetime of planetary scale atmospheric structures. The similarity of scaling breaks observed in all the datasets justify the dependence of scaling break on the value of the largest planetary spatial scale (and its corresponding eddy turnover time or lifetime). All these scaling ranges of both the first and second scaling regimes are tabulated in Table. 4. Henceforth the scaling moment functions of the first and second scaling regime are denoted as  $K_1(q)$  and  $K_2(q)$  respectively.

### 3.2 Double Trace Moment (DTM) Analysis

135 Although the TM analysis helps in estimating  $K(q)$ , it does not provide explicit estimates of UM parameters  $\alpha, C_1$ . To do this the DTM analysis (Lavalée et al., 1993) is used:

$$DTM_\lambda = \lambda^{\eta \alpha K(q)} \quad (5)$$

where  $\eta$  is the power to which the field is raised. Eq. (5) suggests that when  $K(q, \eta)$  vs.  $\eta$  is plotted in log-log coordinates, the slope of a fitted straight line gives the estimate of  $\alpha$ , whereas  $C_1$  is calculated using this  $\alpha$  estimate and the y-intercept of the  
 140 fitted straight line. While performing the usual DTM analysis it is found that the  $\alpha$  estimates are larger than 2 (thereby exceeding the limits in Eq. 2) in the first scaling regime for all the datasets considered here. Generally this could be due to two different issues: (i) an incorrect  $\alpha$  estimation procedure, or (ii) an incorrect assumption about the processes conservativeness. However, for the datasets considered here the first possibility seems more likely due to the fact that the H estimates are negligibly small (as shown in Table. 4 and discussed earlier in section 3) and that Fourier analysis of these datasets are unreliable due to the  
 145 small sample size chosen ( $N_s = 1$ ). Therefore, to overcome this issue an iterative DTM procedure is used here. More technical details about this procedure is given in the Appendix A. Table. 4 shows the UM parameters estimated using the 9 different datasets, while Fig. 4 shows the DTM based estimation procedure. The parameters for the first scaling regime and second scaling regimes are denoted by the subscripts 1 and 2 respectively. Although 3 different scaling breaks and 6 different pairs of  $\alpha, C_1$  values are empirically estimated (3 pairs for each scaling regime) for each region, for simulating a reference rainfall



150 scenario that corresponds to rainfall observed in the corresponding region only 1 scaling break and 2 pairs of  $\alpha, C_1$  values  
 (1 pair for each scaling regime) are necessary (since these values are not too dependent on the dataset used, this choice is  
 justified). The UM parameters estimated from the daily and six-minutes data are selected to be used for the first and second  
 scaling regime in the simulations, whereas the median value of scaling breaks (out of the three scaling breaks estimated from  
 daily, hourly and six-minutes datasets) are chosen. To confirm that this selection procedure does not result in any significant  
 155 difference in the multifractal characteristics of the datasets and the corresponding simulations we compute the Multifractal  
 Comparison Index (MCI) based on the difference in the theoretical maximum observable singularity from a finite-sized sample  
 $\gamma_s$  (Hubert et al., 1993; Douglas and Barros, 2003)

$$\text{MCI} = \frac{1}{6} \sum_{j=1}^3 \sum_{i=1}^2 |\gamma_{s,obs(j)}(i) - \gamma_{s,sel(j)}(i)| \quad (6)$$

based on the difference between UM parameter values observed from datasets and selected for simulations (as indicated by the  
 160 subscripts *obs* and *sel*) with the analytical expression

$$\gamma_s = \frac{C_1 \alpha}{\alpha - 1} \left( \left( \frac{1}{C_1} \right)^{\frac{\alpha-1}{\alpha}} - \frac{1}{\alpha} \right) \quad (7)$$

with respect to  $\alpha$  and  $C_1$ , the indices  $i, j$  denote the scaling regime (first or second) and the dataset (6-minutes, hourly or daily)  
 used respectively.

MCI is computed to be 0.03 for both Paris and Nantes, and 0.04 for Aix. These low values of MCI justify the aforementioned  
 165 selection procedure.

#### 4 Discrete-in-scale Universal Multifractal cascades

Multifractal cascade processes have strongly non-Gaussian statistics (e.g., fat-tailed distributions) and therefore are capable  
 of generating structures of highly varying intensities. These cascades represent the atmospheric physical processes underlying  
 rainfall generation in an abstract (Richardson's idea of energy transfer from large to small scales by random breakups of  
 170 eddies) but explicit manner by the concept of scale-symmetry or scale-invariance (a property respected even by the Navier-  
 Stokes equation used by state-of-the-art NWP models for operational weather forecasting). Therefore, these types of models  
 can be considered as a bridge between purely statistical and purely physical models. Due to their multiplicative property the  
 heterogeneity of the simulated field increase incrementally at smaller scales (making these models capable of generating scale-  
 dependent rain rates as observed in nature). Although discrete-in-scale cascades consider scale-ratios that are integer powers of  
 175 integers they exhibit better scaling properties and are pedagogically straightforward compared to continuous-in-scale cascades  
 (Lovejoy and Schertzer, 2010a, b). Furthermore, for the current purpose of simulating rainfall fields anisotropic and vector  
 generalizations do not seem too relevant. The discrete-in-scale UM cascade model is used here to simulate an ensemble of  
 rainfall scenarios for each region (and its corresponding  $P, D, T$  specifications). The basic idea of discrete-in-scale cascades  
 (Schertzer and Lovejoy, 1989, 2011) is to iteratively divide large-scale eddies (structures) using a constant integer scale ratio





180  $\lambda_1$  (usually 2 as mentioned earlier) and multiplicatively distribute flux ( $\varepsilon_\lambda$ ) to these sub-eddies randomly (stochastically). It is convenient to do this using an additive noise or generator  $\Gamma_\lambda$  (generator) the exponential of which results in the multiplicatively modulated multifractal flux field at resolution  $\lambda$  (Schertzer and Lovejoy, 1989). To simulate universal multifractals (whose statistics are governed by Eqs. 1 and 2) this generator must satisfy

$$\langle \varepsilon_\lambda^q \rangle = \langle e^{q\Gamma_\lambda} \rangle = \lambda^{\frac{C_1}{\alpha-1} q^\alpha} \quad (8)$$

185 To do this an extremal Lévy random variable of index  $\alpha$  and suitable amplitude (Pecknold et al., 1993; Gires et al., 2013) - that is a function of  $C_1$  - is chosen as  $\Gamma_\lambda$  (this generator generates the singularity  $\gamma_\lambda$  corresponding to each sub-eddy). In the present context rainfall  $R_\lambda$  accumulated in a given interval of time is the flux  $\varepsilon_\lambda$ . Such a simulated field when normalized by its ensemble average is canonically conserved (Schertzer and Lovejoy, 2004b).

#### 4.1 Simulating reference rainfall scenarios

190 To have the same  $P, D, T$  characteristics of the reference rainfall, a simulated rainfall series with largest (temporal) scale ( $T_{sim}$ ) needs to have a specific number ( $\rho$ ) of peak values of rainfall ( $\geq P$ ) accumulated over specific durations ( $D$ ) so that their return period  $T = \frac{T_{sim}}{\rho}$ . A simple way to do this is to multiply the simulated multifractal time series (with largest scale  $T_{sim} = \rho T$ ,  $\forall \rho \in Z^+$ ) by an appropriate renormalization constant (RC):  $P$  divided by the  $\rho$ -th highest value in the multifractal series aggregated over duration  $D$ . Therefore, the simulated rainfall series are dependent on these  $P, D, T$  values, resulting in 1  
 195 rainfall series for Paris, 11 rainfall series for Nantes, and 3 rainfall series for Aix. Since the observed datasets have two scaling regimes it is necessary to use a double cascade: a coarser resolution cascade using parameters  $\alpha_1, C_{1_1}$  for the first scaling regime and a finer resolution cascade using parameters  $\alpha_2, C_{1_2}$  for the second scaling regime. Let the smallest scale observed and simulated be  $\delta$  (here  $\delta = 6$  minutes for all three regions). The largest temporal scale selected from observed datasets  $T_{sel}$  is related to the largest scale that can be simulated  $T_{(s, sim)}$  (largest scale in simulated sample which is a power of  $\lambda_1 = 2$  and  
 200  $\leq T_{sim}$ ):

$$T_{s, sim} = \delta 2^{\lfloor \log_2 \frac{T_{sel}}{\delta} \rfloor}; \quad T_{s, sim} \leq T_{sim} \quad (9)$$

where  $\lfloor x \rfloor$  denotes the integer part of  $x$ .

The coarse resolution cascade produces a multifractal time series  $\varepsilon_{\lambda_B}$  where  $\lambda_B = \left( \frac{T_{s, sim}}{T_{B, sim}} \right)$  and  $T_{B, sim} = \delta 2^{\lfloor \log_2 \frac{T_{sel}}{\delta} \rfloor}$  is the simulated scaling break. Each rainfall value of this coarse resolution multifractal series is now the parent structure of the  
 205 second (fine resolution) cascade that proceeds from  $T_{B, sim}$  up to  $\delta$ . A multifractal time series  $\varepsilon_{\lambda_\delta}$  where  $\lambda_\delta = \frac{T_{s, sim}}{\delta}$  is thus finally produced by the double cascade simulation (DCS). The DCS is repeated a sufficient number of times (if  $T_{s, sim} < T_{sim}$ ) to finally extract a time series  $\varepsilon_{\Lambda_\delta}$  where  $\Lambda_\delta = \frac{T_{sim}}{\delta}$  (here  $\delta = 6$  minutes). The  $\rho$ -th highest value in a aggregated multifractal series  $\bar{\varepsilon}$  ( $\varepsilon_{\Lambda_\delta}$  aggregated to resolution  $\frac{T_{sim}}{D}$ ) when multiplied by RC should equal  $P$ . If we rank the values in series  $\bar{\varepsilon}$  in decreasing order and call it  $\bar{\varepsilon}_{DO}$ , then the  $\rho$ -th value  $\bar{\varepsilon}_{DO}(\rho)$  is the  $\rho$ -th highest value. Therefore,  $RC$  is computed as

$$210 \quad RC = \frac{P}{\bar{\varepsilon}_{DO}(\rho)} \quad (10)$$





The  $RC$  computed using Eq. (10) when multiplied to  $\varepsilon_{\Lambda_\delta}$  gives the final rainfall series that has characteristics corresponding to the reference rainfall. This entire procedure is repeated  $n_e$  times to generate an  $n_e$  member ensemble of possible reference rainfall scenarios (Fig. 5. schematically presents the whole simulation method). Here  $n_e = 10$ , i.e. an ensemble of 10 members (m1 to m10) are simulated.

215 Figure. 6 shows the reference rainfall simulations for Paris: both rainfall data and singularities can be compared from the figure. The maximum observed and simulated singularities are closer to each other than that of corresponding rainfall values. This may be attributed to the fact that singularities are less scale-dependent than rainfall and the observed and simulated rainfall have different scale ratios (resulting in the unreliability of comparison using parameters that are more scale dependent) since their largest scales are different in spite of their smallest scales being equal. Figure. 6 e) shows that the simulated rainfall (from  
220 one member of the ensemble: m10) obey the  $P, D, T$  reference criterion for Paris region. To highlight the internal variability of the 10 reference rainfall scenarios simulated, events where exactly  $P$  mm rainfall occur within  $D$  hours duration are plotted separately in Figure. 6 f). Figures. 7 and 8 are the same as Fig. 6 f) but are for the different  $P, D, T$  specifications of Nantes and Aix-en-Provence.

## 4.2 Comparing simulations with observational datasets

225 Four metrics possessing different properties have been defined to compare the stochastic simulations of rainfall to the actual datasets. The first metric is the Multifractal Comparison Metric (MCM), the second metric is the Rainfall Comparison Metric (RCM), the third metric is the Singularity Comparison Metric (SCM), whereas the fourth and final metric is the Codimension Comparison Metric (CCM). These metrics are defined with the general idea that lower metrics correspond to better simulations and vice-versa.

### 230 4.2.1 Multifractal Comparison Metric (MCM)

The MCM is a theoretical metric and is computed based on the maximum observable theoretical singularity  $\gamma_s$  (Eq. 7) from a finite sample size  $N_s \approx \lambda^{D_s}$  where  $D_s$  is the sample dimension (Schertzer and Lovejoy, 1992) in each dataset and in each simulated member of the ensemble

$$\text{MCM} = \frac{1}{6} \sum_{j=1}^3 \sum_{i=1}^2 \left| \gamma_{s,obs}(i) - \frac{1}{10} \sum_{k=1}^{10} \gamma_{s,sim(k)}(i) \right| \quad (11)$$

235 where  $j$  indicates the dataset used (daily, hourly or 6 minute),  $i$  denotes the scaling regime (first or second),  $k$  indicates the ensemble member. MCM is closely related to MCI defined earlier, the only difference between them is that MCM uses the UM parameters estimated from DTM analysis of simulated members, whereas MCI directly uses the UM parameters selected for simulations from the observed datasets. Therefore, as expected the MCM computed for all the simulations are very low (shown in Figure. 9) and close to MCI. Since both MCM and MCI depend only on the UM parameters (or in other words the  
240 multifractal characteristics of the series), they are scale-independent (this means that MCM of two fields of same or different resolutions or lengths are not too different). Since renormalization does not affect the multifractal properties of a series, the



MCM is independent of  $P, D, T$ . Lower values of MCM imply that the simulation has multifractal properties close to that of observed data.

#### 4.2.2 Rainfall Comparison Metric (RCM)

245 RCM on the other hand is a more practical metric and is computed based on the highest rainfall value present in the dataset and in each simulation member:

$$\text{RCM} = \frac{1}{3} \sum_{j=1}^3 \frac{\left| \max[R_{\Lambda(\text{obs}(j))}] - \frac{1}{10} \sum_{k=1}^{10} \max[R_{\Lambda(\text{sim}(k), j)}] \right|}{\max[R_{\Lambda(\text{obs}(j))}]} \quad (12)$$

where  $\Lambda(\text{obs}(j)) = \frac{L_{\text{obs}(j)}}{\delta(j)}$ ;  $\Lambda(\text{sim}(k), j) = \frac{L_{\text{sim}(k)}}{\delta(j)}$ ;  $\delta(j) = 1 \text{ day}, 1 \text{ hour}, 6 \text{ minutes}$  for  $j = 1, 2, 3$ , the indices  $j, k$  have the same meaning as in MCM.

250 Lower values of RCM imply that the extreme behaviour of simulations are closer to that of the observed data. But RCM is sensitively dependent on scale and  $P, D, T$ . Therefore, as shown in Figure. 9 the RCM values are larger for cases where  $\frac{P}{D}$  is larger. This might be due to the fact that the datasets used (since they are of shorter lengths) are not actually representative of these specific  $P, D, T$  values that correspond to rainfall events that are more extreme (since probability of observing rarer events is higher in larger datasets).

#### 255 4.2.3 Singularity Comparison Metric (SCM)

SCM is a metric that instead of comparing the actual fields compares the singularities corresponding to them, and is computed as:

$$\text{SCM} = \frac{1}{3} \sum_{j=1}^3 \frac{\left| \max[\gamma_{\Lambda(\text{obs}(j))}] - \frac{1}{10} \sum_{k=1}^{10} \max[\gamma_{\Lambda(\text{sim}(k), j)}] \right|}{\max[\gamma_{\Lambda(\text{obs}(j))}]} \quad (13)$$

where  $\gamma_{\Lambda(\text{obs}(j))} = \frac{\log R_{\Lambda(\text{obs}(j))}}{\log \Lambda(\text{obs}(j))}$ ;  $\gamma_{\Lambda(\text{sim}(k), j)} = \frac{\log R_{\Lambda(\text{sim}(k), j)}}{\log \Lambda(\text{sim}(k), j)}$ , the indices  $j, k$  have the same meaning as in MCM.

260 Lower values of SCM imply that the simulations are closer to the observations (after reducing the effect of scale-dependence on the comparison) since the singularities corresponding to the simulations and the singularities corresponding to the observations are close to each other. Although SCM is scale-dependent it is less sensitive to scale than RCM; moreover SCM is also dependent on  $P, D, T$ . Therefore, SCM values of all simulations are low ( $\leq 0.15$ ) even for cases where  $\frac{P}{D}$  is larger as shown in Figure. 9.

#### 265 4.2.4 Codimension Comparison Metric (CCM)

The main drawback of the MCM, RCM and SCM are that they focus only on either the maximum rainfall values or the maximum singularities. On the contrary, a range of values rather than threshold values can be used. For instance, the codimension of singularity  $c(\gamma)$  takes into account a range of singularities larger than  $\gamma$ . Following Schertzer and Lovejoy 1987:

$$\text{Pr}[R_{\lambda} \geq \lambda^{\gamma}] \approx \lambda^{-c(\gamma)} \quad (14)$$



270 meaning that  $c(\gamma)$  can be obtained as the negative of the slope of a straight line fitted to log-log plot of  $\Pr[R_\lambda \geq \lambda^\gamma]$  with respect to  $\lambda$ . Equation. 14 (where  $\approx$  indicates an asymptotic equivalence) implies that  $c(\gamma)$  is almost scale independent and any metric defined using it should also be not very scale-sensitive. The CCM is defined as

$$\text{CCM} = \frac{1}{3n} \sum_{j=1}^3 \sum_{i=1}^n \left| c_{obs(j)}(\gamma_{\Lambda(obs(j))}(i)) - \frac{1}{10} \sum_{k=1}^{10} c_{sim(j,k)}(\gamma_{\Lambda(obs(j))}(i)) \right| \quad (15)$$

275 where  $\gamma_{\Lambda(obs(j))}(i) = \min[\gamma_{\Lambda(obs(j))}] + \frac{1}{n}(i-1)(\max[\gamma_{\Lambda(obs(j))}] - \min[\gamma_{\Lambda(obs(j))}])$ , the indices  $j, k$  have the same meaning as in MCM, whereas  $i$  indexes the singularities (here  $n = 10$  singularities are used for the comparison procedure).

The CCM is dependent on  $P, D, T$  via the singularities  $\gamma_\Lambda$ , therefore in an almost scale-independent manner. As shown in Fig. 9, the SCM and CCM values are consistently low implying that it is possible to simulate reference rainfall ensembles characterized by the required properties  $(P, D, T)$  while taking into account temporal variability.

## 5 Conclusions

280 A novel method is proposed to simulate reference rainfall scenarios that are indispensable for hydrological applications such as designing green roofs and other generic storm-water management devices. The suggested discrete-in-scale Universal Multifractal cascade based method is used here to stochastically simulate an ensemble of reference rainfall scenarios (with rainfall events exceeding or equal to  $P$  mm within  $D$  hours duration having a return period of  $T$  years) as specified by regional storm-water management regulations for three conurbations in France. The extreme variability of  $P, D, T$  values which is a direct  
 285 result of the extreme space-time variability of precipitation and underlying atmospheric processes, not only justifies but also makes the choice of UM framework rather crucial in producing computationally cheap, physically realistic reference rainfall ensembles. Furthermore, four new metrics are proposed to quantify the performance of the suggested procedure and analyse their effectiveness. Three (MCM, SCM and CCM) out of the four metrics (which are not too scale-dependent) seem to indicate that the simulations are good. CCM being almost scale-independent, and utilizing a range of values rather than just maxima  
 290 for comparison seems to be the most reliable comparison metric. Therefore, the consistently low CCMs show that the proposed method is indeed an attractive choice to stochastically simulate physically-based reference rainfall scenarios. Although only purely temporal, discrete-in-scale, conservative simulations over three locations (Paris, Nantes, Aix) are considered in this study, this approach could possibly be generalized to spatio-temporal, continuous-in-scale, non-conservative simulations over other locations as well. Finally, it is worth noting that the suitability of the UM framework in simulating reference rain-  
 295 fall scenarios and in several other geophysical applications (Ramanathan et al., 2018, 2019; Ramanathan and Satyanarayana, 2019, 2021; Ramanathan et al., 2021), illustrates that this generalized, physically based, computationally simple framework could probably be ideal for framing reference rainfall regulations guiding hydrological applications/designs.



## Appendix A

To get more accurate  $\alpha$  estimates for the first scaling regime an iterative DTM procedure is implemented here. Following earlier studies (Hoang et al., 2012) the idea of this procedure is to estimate  $\eta_{\min} = (\frac{C_{\Sigma}}{C_1})^{\frac{1}{\alpha}} \max[1, \frac{1}{q}]$  and  $\eta_{\max} = (\frac{1}{C_1})^{\frac{1}{\alpha}} \min[1, \frac{1}{q}]$ : first using an initial guess of  $\alpha, C_1$  (based on initial guesses of  $\eta_{\min}$  and  $\eta_{\max}$ ) then subsequent  $\eta$  range and  $\alpha, C_1$  estimates are obtained in each iteration until there is no longer any change in the  $\eta$  range and therefore the  $\alpha, C_1$  estimates. The codimension (difference between the dimension of the embedding space and that of the dimension of the set under consideration) of non-zero rainfall support  $C_{\Sigma} = 1 - D_{\Sigma}$  (here  $D_{\Sigma}$  is the fractal dimension of rainfall greater than the minimum threshold considered). However, the procedure used here is slightly modified: instead of searching for both  $\eta_{\min}$  and  $\eta_{\max}$  simultaneously in each iteration, the current procedure fixes  $\eta_{\min}$  as a constant value (here it is initially 1) and obtains different  $\eta_{\max}, \alpha, C_1$  values in each iteration. If the  $\alpha$  estimate is still  $> 2$  or if the  $\alpha$  values keep changing even after a certain number of iterations,  $\eta_{\min}$  is slightly reduced and the whole procedure is repeated. A  $q$  value of 0.8 is used here so that the usable range of  $\eta$  is larger (since the multifractal phase transition due to divergence of moments is more delayed) resulting in more reliable  $\alpha, C_1$  estimates.

*Author contributions.* A.R. performed the study and prepared the manuscript, P.A.V. and D.S. supervised the work, I.T. provided vital suggestions, R.P. and L.S. helped in gaining insights into commercial hydro-meteorological applications

*Competing interests.* The authors declare that no competing interests are present

*Acknowledgements.* The first author acknowledges SOPREMA for funding his post-doctoral research at HM&Co, ENPC. The authors acknowledge MeteoFrance for providing insitu rainfall observational datasets used in this study.



## 315 References

- Arnaud, P. and Lavabre, J.: Nouvelle approche de la prédétermination des pluies extrêmes, *Comptes Rendus de l'Académie des Sciences - Series IIA - Earth and Planetary Science*, 328, 615–620, [https://doi.org/10.1016/S1251-8050\(99\)80158-X](https://doi.org/10.1016/S1251-8050(99)80158-X), 1999.
- Brandsma, T. and Buishand, T. A.: Simulation of extreme precipitation in the Rhine basin by nearest-neighbour resampling, *Hydrology and Earth System Sciences*, 2, 195–209, <https://doi.org/https://doi.org/10.5194/hess-2-195-1998>, publisher: Copernicus GmbH, 1998.
- 320 Burian, S. J., Durrans, S. R., Nix, S. J., and Pitt, R. E.: Training Artificial Neural Networks to Perform Rainfall Disaggregation, *Journal of Hydrologic Engineering*, 6, 43–51, [https://doi.org/10.1061/\(ASCE\)1084-0699\(2001\)6:1\(43\)](https://doi.org/10.1061/(ASCE)1084-0699(2001)6:1(43)), publisher: American Society of Civil Engineers, 2001.
- Cameron, D., Beven, K., and Tawn, J.: Modelling extreme rainfalls using a modified random pulse Barlett-Lewis stochastic rainfall model (with uncertainty), *Advances in Water Resources*, [https://doi.org/10.1016/S0309-1708\(00\)00042-7](https://doi.org/10.1016/S0309-1708(00)00042-7), 2000a.
- 325 Cameron, D., Beven, K., and Tawn, J.: An evaluation of three stochastic rainfall models, *Journal of Hydrology*, [https://doi.org/10.1016/S0022-1694\(00\)00143-8](https://doi.org/10.1016/S0022-1694(00)00143-8), 2000b.
- Cowpertwait, P. S.: Generalized point process model for rainfall, *Proceedings of The Royal Society of London, Series A: Mathematical and Physical Sciences*, <https://doi.org/10.1098/rspa.1994.0126>, 1994.
- Cowpertwait, P. S. P., O'Connell, P. E., Metcalfe, A. V., and Mawdsley, J. A.: Stochastic point process modelling of rainfall. II. Regionalisation and disaggregation, *Journal of Hydrology*, 175, 47–65, [https://doi.org/10.1016/S0022-1694\(96\)80005-9](https://doi.org/10.1016/S0022-1694(96)80005-9), 1996.
- 330 Douglas, E. M. and Barros, A. P.: Probable Maximum Precipitation Estimation Using Multifractals: Application in the Eastern United States, *Journal of Hydrometeorology*, 4, 1012–1024, [https://doi.org/10.1175/1525-7541\(2003\)004<1012:PMPEUM>2.0.CO;2](https://doi.org/10.1175/1525-7541(2003)004<1012:PMPEUM>2.0.CO;2), publisher: American Meteorological Society Section: *Journal of Hydrometeorology*, 2003.
- Gires, A., Tchiguirinskaia, I., Schertzer, D., and Lovejoy, S.: Development and analysis of a simple model to represent the zero rainfall in a universal multifractal framework, *Nonlinear Processes in Geophysics*, <https://doi.org/10.5194/npg-20-343-2013>, 2013.
- 335 Gyasi-Agyei, Y. and Willgoose, G. R.: Generalisation of a hybrid model for point rainfall, *Journal of Hydrology*, [https://doi.org/10.1016/S0022-1694\(99\)00054-2](https://doi.org/10.1016/S0022-1694(99)00054-2), 1999.
- Hoang, C. T., Tchiguirinskaia, I., Schertzer, D., Arnaud, P., Lavabre, J., and Lovejoy, S.: Assessing the high frequency quality of long rainfall series, *Journal of Hydrology*, <https://doi.org/10.1016/j.jhydrol.2012.01.044>, 2012.
- 340 Hoang, C. T., Tchiguirinskaia, I., Schertzer, D., and Lovejoy, S.: Caractéristiques multifractales et extrêmes de la précipitation à haute résolution, application à la détection du changement climatique, *Revue des Sciences de l'Eau*, <https://doi.org/10.7202/1027806ar>, 2014.
- Hubert, P., Tessier, Y., Lovejoy, S., Schertzer, D., Schmitt, F., Ladoy, P., Carbonnel, J. P., Violette, S., and Desuroisne, I.: Multifractals and extreme rainfall events, *Geophysical Research Letters*, 20, 931–934, <https://doi.org/10.1029/93GL01245>, \_eprint: <https://onlinelibrary.wiley.com/doi/pdf/10.1029/93GL01245>, 1993.
- 345 Ladoy, P., Schmitt, F., Schertzer, D., and Lovejoy, S.: The multifractal temporal variability of Nimes rainfall data, *Comptes Rendus - Academie des Sciences, Serie II*, 1993.
- Lavallee, D., Lovejoy, S., Schertzer, D., and Ladoy, P.: Nonlinear variability of landscape topography: multifractal analysis and simulation, *Fractals in geography*, 1993.
- Lovejoy, S. and Schertzer, D.: Multifractals, cloud radiances and rain, *Journal of Hydrology*, 322, 59–88, <https://doi.org/10.1016/j.jhydrol.2005.02.042>, 2006.
- 350



- Lovejoy, S. and Schertzer, D.: Scale, scaling and multifractals in geophysics: twenty years on, in: *Nonlinear dynamics in geosciences*, pp. 311–337, doi: 10.1007/978-0-387-34918-3-18, 2007.
- Lovejoy, S. and Schertzer, D.: On the simulation of continuous in scale universal multifractals, part I: Spatially continuous processes, *Computers and Geosciences*, 36, 1393–1403, <https://doi.org/10.1016/j.cageo.2010.04.010>, 2010a.
- 355 Lovejoy, S. and Schertzer, D.: On the simulation of continuous in scale universal multifractals, Part II: Space-time processes and finite size corrections, *Computers and Geosciences*, 36, 1404–1413, <https://doi.org/10.1016/j.cageo.2010.07.001>, 2010b.
- Lovejoy, S. and Schertzer, D.: *The Weather and Climate: Emergent Laws and Multifractal Cascades*, Cambridge University Press, Cambridge, <http://ebooks.cambridge.org/ref/id/CBO9781139093811>, page: 491 container-title: *The Weather and Climate: Emergent Laws and Multifractal Cascades* DOI: 10.1017/CBO9781139093811, 2013.
- 360 Mellor, D.: The modified turning bands (MTB) model for space-time rainfall. I. Model definition and properties, *Journal of Hydrology*, 175, 113–127, [https://doi.org/10.1016/S0022-1694\(96\)80008-4](https://doi.org/10.1016/S0022-1694(96)80008-4), 1996.
- Onof, C., Chandler, R. E., Kakou, A., Northrop, P., Wheeler, H. S., and Isham, V.: Rainfall modelling using poisson-cluster processes: A review of developments, *Stochastic Environmental Research and Risk Assessment*, <https://doi.org/10.1007/s004770000043>, 2000.
- Pecknold, S., Lovejoy, S., Schertzer, D., Hooge, C., and Malouin, J. F.: *The simulation of universal multifractals*, pp. 228–267, World Scientific, 1993.
- 365 Pegram, G. G. S. and Clothier, A. N.: High resolution space–time modelling of rainfall: the “String of Beads” model, *Journal of Hydrology*, 241, 26–41, [https://doi.org/10.1016/S0022-1694\(00\)00373-5](https://doi.org/10.1016/S0022-1694(00)00373-5), 2001.
- Qiu, Y., da Silva Rocha Paz, I., Chen, F., Versini, P.-A., Schertzer, D., and Tchiguirinskaia, I.: Space variability impacts on hydrological responses of nature-based solutions and the resulting uncertainty: a case study of Guyancourt (France), *Hydrology and Earth System Sciences*, 25, 3137–3162, <https://doi.org/10.5194/hess-25-3137-2021>, 2021.
- 370 Rajagopalan, B. and Lall, U.: A k-nearest-neighbor simulator for daily precipitation and other weather variables, *Water Resources Research*, 35, 3089–3101, <https://doi.org/https://doi.org/10.1029/1999WR900028>, 1999.
- Ramanathan, A. and Satyanarayana, A.: Higher-order statistics based multifractal predictability measures for anisotropic turbulence and the theoretical limits of aviation weather forecasting, *Scientific Reports*, 9, 19 829, <https://doi.org/10.1038/s41598-019-56304-2>, 2019.
- 375 Ramanathan, A. and Satyanarayana, A. N. V.: Satellite-Based Estimate of Intrinsic Predictability Limits at Convective Scales Over Northeast India, *Earth and Space Science*, 8, e2019EA000 797, <https://doi.org/https://doi.org/10.1029/2019EA000797>, \_eprint: <https://agupubs.onlinelibrary.wiley.com/doi/pdf/10.1029/2019EA000797>, 2021.
- Ramanathan, A., Satyanarayana, A. N. V., and Mandal, M.: Anisotropic Continuous-in-Scale Universal Multifractal Cascades: Simulation, Analysis and Correction Methods, *Mathematical Geosciences*, 50, 827–859, <https://doi.org/10.1007/s11004-018-9746-x>, 2018.
- 380 Ramanathan, A., Satyanarayana, A., and Mandal, M.: Theoretical Predictability Limits of Spatially Anisotropic Multifractal Processes: Implications for Weather Prediction, *Earth and Space Science*, 6, 1067–1080, <https://doi.org/10.1029/2018EA000528>, 2019.
- Ramanathan, A., Versini, P.-A., Schertzer, D., Tchiguirinskaia, I., Perrin, R., and Sindt, L.: Simulating reference rainfall scenarios for hydrological applications using a multifractal approach, Tech. Rep. EGU21-6605, Copernicus Meetings, <https://doi.org/10.5194/egusphere-egu21-6605>, conference Name: EGU21, 2021.
- 385 Salas, J.: *Analysis and modeling of hydrologic time series*, Handbook of hydrology, 1993.
- Schertzer, D. and Lovejoy, S.: Physical modeling and analysis of rain and clouds by anisotropic scaling multiplicative processes, *Journal of Geophysical Research*, 92, 9693–9693, <https://doi.org/10.1029/JD092iD08p09693>, 1987.



- Schertzer, D. and Lovejoy, S.: Multifractal simulations and analysis of clouds by multiplicative processes, *Atmospheric Research*, 21, 337–361, [https://doi.org/10.1016/0169-8095\(88\)90035-X](https://doi.org/10.1016/0169-8095(88)90035-X), 1988.
- 390 Schertzer, D. and Lovejoy, S.: Nonlinear Variability in Geophysics: Multifractal Simulations and Analysis, in: *Fractals' Physical Origin and Properties*, DOI: 10.1007/978-1-4899-3499-4-3, 1989.
- Schertzer, D. and Lovejoy, S.: Hard and soft multifractal processes, *Physica A: Statistical Mechanics and its Applications*, 185, 187–194, [https://doi.org/10.1016/0378-4371\(92\)90455-Y](https://doi.org/10.1016/0378-4371(92)90455-Y), 1992.
- Schertzer, D. and Lovejoy, S.: Universal Multifractals Do Exist!: Comments on “A Statistical Analysis of Mesoscale Rain-  
395 fall as a Random Cascade”, *Journal of Applied Meteorology and Climatology*, 36, 1296–1303, [https://doi.org/10.1175/1520-0450\(1997\)036<1296:UMDECO>2.0.CO;2](https://doi.org/10.1175/1520-0450(1997)036<1296:UMDECO>2.0.CO;2), publisher: American Meteorological Society section: *Journal of Applied Meteorology and Climatology*, 1997.
- Schertzer, D. and Lovejoy, S.: Space – time complexity and multifractal predictability, *physica A*, 338, 173–186, <https://doi.org/10.1016/j.physa.2004.04.032>, 2004a.
- 400 Schertzer, D. and Lovejoy, S.: Uncertainty and predictability in geophysics: Chaos and multifractal insights, in: *Geophysical Monograph Series*, vol. 150, pp. 317–334, DOI: 10.1029/150GM25, 2004b.
- Schertzer, D. and Lovejoy, S.: MULTIFRACTALS, GENERALIZED SCALE INVARIANCE AND COMPLEXITY IN GEOPHYSICS, *International Journal of Bifurcation and Chaos*, 21, 3417–3456, <https://doi.org/10.1142/S0218127411030647>, 2011.
- SCHERTZER, D., LOVEJOY, S., Lavallee, D., and Schmitt, F.: Universal hard multifractal turbulence: theory and observation, in: *Nonlinear  
405 Dynamics of Structures*, pp. 213–235, World Scientific, in r. z. sagdeev, u. frisch, a. s. moiseev and a. erokhin, eds., edn., 1991.
- Schertzer, D., Tchiguirinskaia, I., Lovejoy, S., and Hubert, P.: No monsters, no miracles: in nonlinear sciences hydrology is not an outlier!, *Hydrological Sciences Journal*, 55, 965–979, <https://doi.org/10.1080/02626667.2010.505173>, 2010.
- Shah, S., O'Connell, P., and Hosking, J.: Modelling the effects of spatial variability in rainfall on catchment response. I. Formulation and calibration of a stochastic rainfall field model, *Journal of Hydrology*, 175, 67–88, [https://doi.org/10.1016/S0022-1694\(96\)80006-0](https://doi.org/10.1016/S0022-1694(96)80006-0), 1996.
- 410 Tessier, Y., Lovejoy, S., and Schertzer, D.: Universal Multifractals: Theory and Observations for Rain and Clouds, *Journal of Applied Meteorology*, 32, 223–250, [https://doi.org/10.1175/1520-0450\(1993\)032<0223:UMTAOF>2.0.CO;2](https://doi.org/10.1175/1520-0450(1993)032<0223:UMTAOF>2.0.CO;2), 1993.
- Tessier, Y., Lovejoy, S., Hubert, P., Schertzer, D., and Pecknold, S.: Multifractal analysis and modeling of rainfall and river flows and scaling, causal transfer functions, *Journal of Geophysical Research Atmospheres*, <https://doi.org/10.1029/96jd01799>, 1996.
- Wheater, H. S., Wheeler, H. S., Isham, V. S., Cox, D. R., Chandler, R. E., Kakou, A., Northrop, P. J., Oh, L., Onof, C., and Rodriguez-Iturbe,  
415 I.: Spatial-temporal rainfall fields: modelling and statistical aspects, <https://doaj.org>, iSSN: 1027-5606, 1607-7938 issue: 4 page: 581-601  
publisher: Copernicus Publications volume: 4, 2000.
- Wilks, D. S.: Multisite generalization of a daily stochastic precipitation generation model, *Journal of Hydrology*, [https://doi.org/10.1016/S0022-1694\(98\)00186-3](https://doi.org/10.1016/S0022-1694(98)00186-3), 1998.





**Table 1.** Comparison of different stochastic rainfall modelling procedures based on literature.

Models	Desirable Features	# of Parameters	References
Simple point process	Computational simplicity	5	Salas (1993)
Cluster processes	Computational simplicity	$\geq 5$	Cowpertwait (1994); Cameron et al. (2000a, b)
Hybrid processes	Computational simplicity	$> 5$	Gyasi-Agyei and Willgoose (1999); Onof et al. (2000)
SHYPRE	Heterogeneity, Extreme statistics, Computational simplicity	8	Arnaud and Lavabre (1999)
SHYREG	Computational simplicity	3	
Markov chain	Non-stationarity, Heterogeneity, Computational simplicity	4	Wilks (1998)
Non-parametric	Extremal statistics, Nonstationary, Heterogeneity	0	Rajagopalan and Lall (1999); Brandsma and Buishand (1998)
Point models	Computational simplicity	$\geq 5$	Cowpertwait et al. (1996)
Artificial neural networks	-	Varies	Burian et al. (2001)
Cell cluster	Computational simplicity	7	Wheater et al. (2000)
Modified Turning Band	Computational simplicity	8	Mellor (1996)
Radar-based bead	Heterogeneity, Scale symmetry, Extremal statistics, Nonstationary, Computational simplicity	4	Pegram and Clothier (2001)
Nonhomogeneous random cascade	Heterogeneity, Scale symmetry, Nonlinearity, Space-time complexity, Extremal statistics, Nonstationary, Computational simplicity	2	Schertzer and Lovejoy (1988, 1989, 2004a, b)



**Table 2.** Variability of reference rainfall regulations in the three regions considered by this study.

<b>Region</b>	<b>Duration <math>D</math> (hours)</b>	<b>Return period <math>T</math> (years)</b>	<b>Precipitation <math>P</math> (mm)</b>
Paris	4	0.5	16
Nantes	1	$\frac{1}{12}$	6
	1	2	16
	1,12,24	10	29,48,56
	1,12,24	30	41,61,68
	1,12,24	50	49,69,75
Aix-en-Provence	2	30	100
	2	50	120
	2	100	160



**Table 3.** Resolution, Length and Percentage of Missing data of rainfall datasets used in this study.

<b>Region</b>	<b>Dataset (resolution)</b>	<b>Length <math>L_{obs}</math> (years)</b>	<b>% Missing</b>
Paris	PD1 (daily)	100 (1921 - 2020)	0
	PD2 (hourly)	28 (1993 - 2020)	0.3
	PD3 (6 minutes)	15 (2006 - 2020)	0.6
Nantes	ND1 (daily)	75 (1946 - 2020)	0
	ND2 (hourly)	28 (1986,1994 - 2020)	0.7
	ND3 (6 minutes)	15 (2006 - 2020)	0.1
Aix-en-Provence	AD1 (daily)	60 (1961 - 2020)	0
	AD2 (hourly)	28 (1993 - 2020)	0.7
	AD3 (6 minutes)	15 (2006 - 2020)	0.17



**Table 4.** UM parameter estimates for first and second scaling regimes from different datasets (PD1 to AD3), the scaling regimes and parameters selected for simulating rainfall over each corresponding region.  $H$  values are not included in the selected parameters and assumed to be zero since these rain fields seem to be almost conservative (both  $H_1$  and  $H_2$  are close to zero).

Region	Dataset	Scaling Regimes	$\alpha_1,$	$C_{1_1},$	$H_1,$	Selected for simulations		
			$\alpha_2$	$C_{1_2}$	$H_2$	Scaling Regimes	$\alpha_1,$ $\alpha_2$	$C_{1_1},$ $C_{1_2}$
Paris	PD3	15 years - 17 days	1.97	0.03	-0.00002	100 years - 21 days	1.89	0.02
		17 days - 6 mins	0.56	0.45	0.002	21 days - 6 mins	0.56	0.45
	PD2	28 years - 21 days	1.84	0.03	0.0002			
		21 days - 1 hour	0.55	0.48	-0.003			
	PD1	100 years - 32 days	1.89	0.02	0.00008			
		32 days - 1 day	0.71	0.37	-0.0007			
Nantes	ND3	15 years - 17 days	1.85	0.03	0.002	75 years - 21 days	1.7	0.02
		17 days - 6 mins	0.69	0.38	0.002	21 days - 6 mins	0.69	0.38
	ND2	28 years - 21 days	1.86	0.02	0.0002			
		21 days - 1 hour	0.59	0.42	-0.0007			
	ND1	75 years - 32 days	1.7	0.02	0.00008			
		32 days - 1 day	0.65	0.35	0.002			
Aix-en-Provence	AD3	15 years - 34 days	1.79	0.04	0.00008	60 years - 32 days	1.8	0.03
		34 days - 6 mins	0.51	0.48	0.0035	32 days - 6 mins	0.51	0.48
	AD2	28 years - 21 days	1.76	0.06	-0.00007			
		21 days - 1 hour	0.48	0.55	0.005			
	AD1	60 years - 32 days	1.8	0.03	-0.0003			
		32 days - 1 day	0.49	0.54	0.0002			

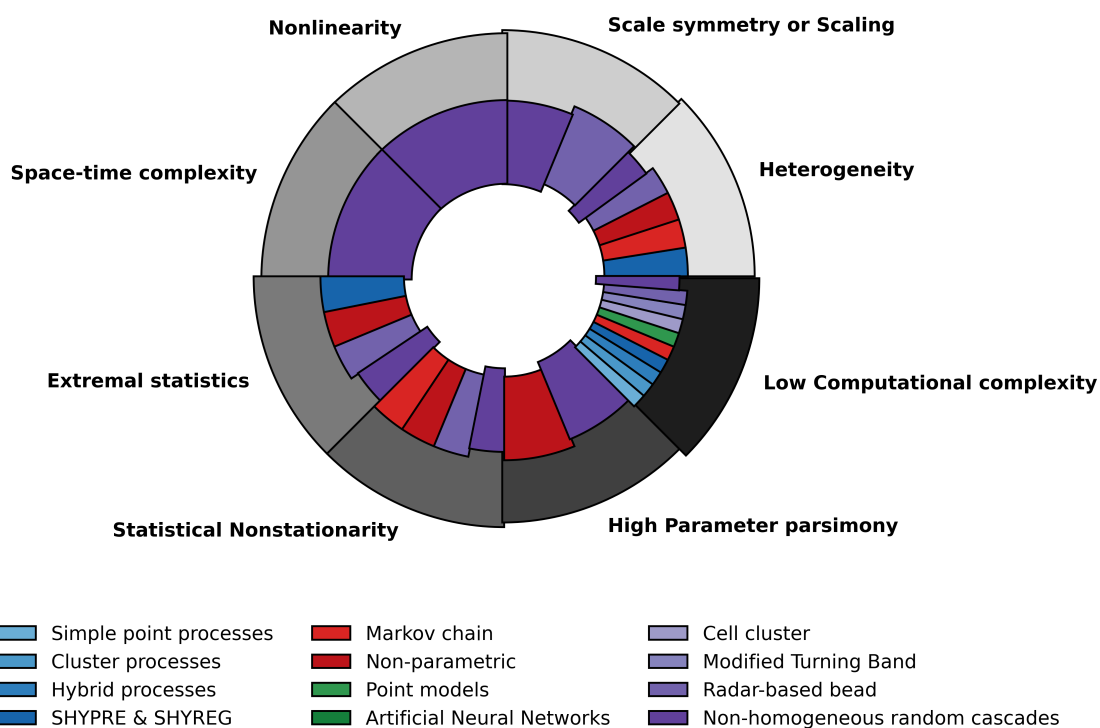


**Figure 1.** Outer-ring: Desirable characteristics in stochastic high-resolution rainfall simulation models. Inner-ring: Models that possess these characteristics (based on Table 1). Models with  $\leq 3$  parameters are considered here to possess High Parameter parsimony. Non-homogeneous random cascade models seem to possess all the desirable properties.

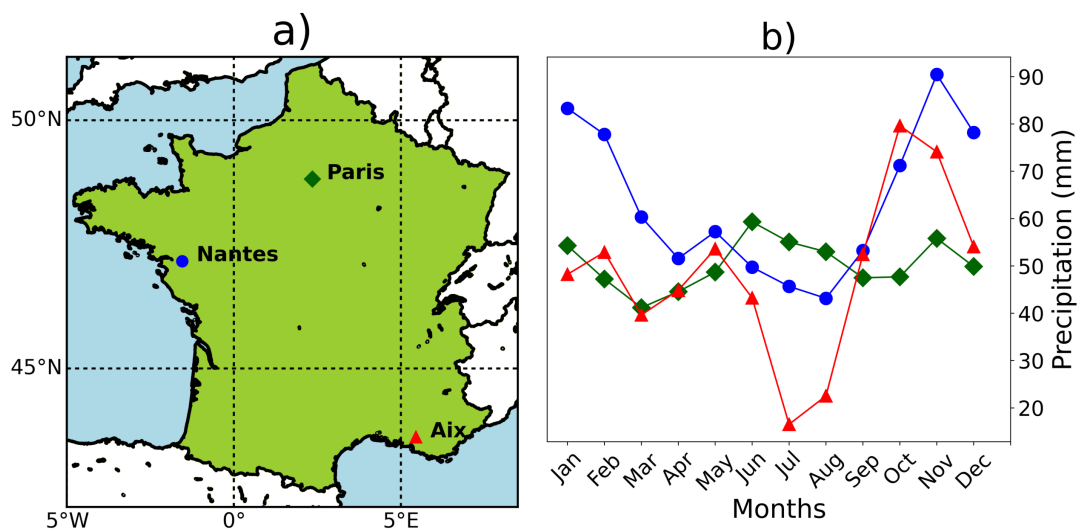


**Figure 2.** a) The three chosen cities/conurbations in mainland France, and b) their monthly cumulative precipitation climatology (using PD1, ND1 and AD1 datasets).

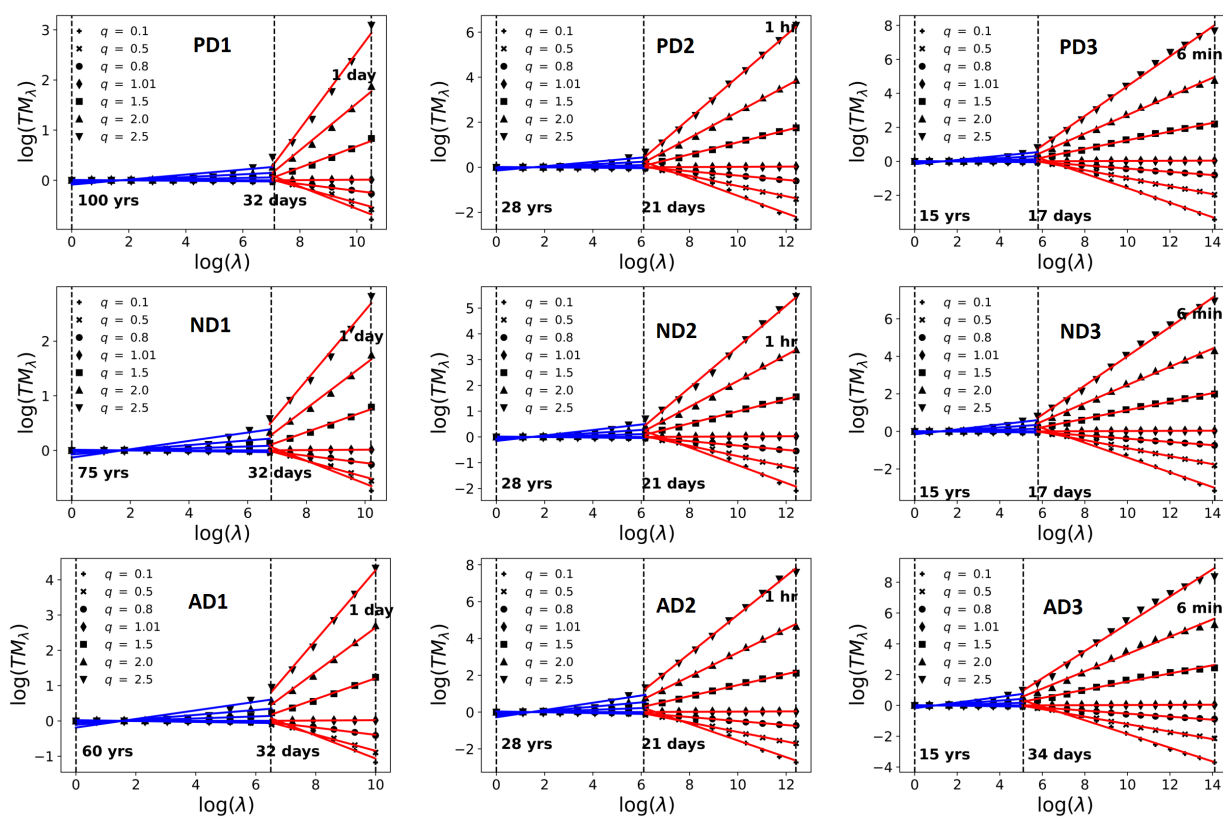


**Figure 3.** Trace Moment Analysis of accumulated rainfall data. Top Row: Paris: PD1, PD2, PD3; Middle Row: Nantes: ND1, ND2, ND3, and Bottom Row: Aix: AD1, AD2, AD3. The first scaling regime is shown in blue whereas the second scaling regime is shown in red.



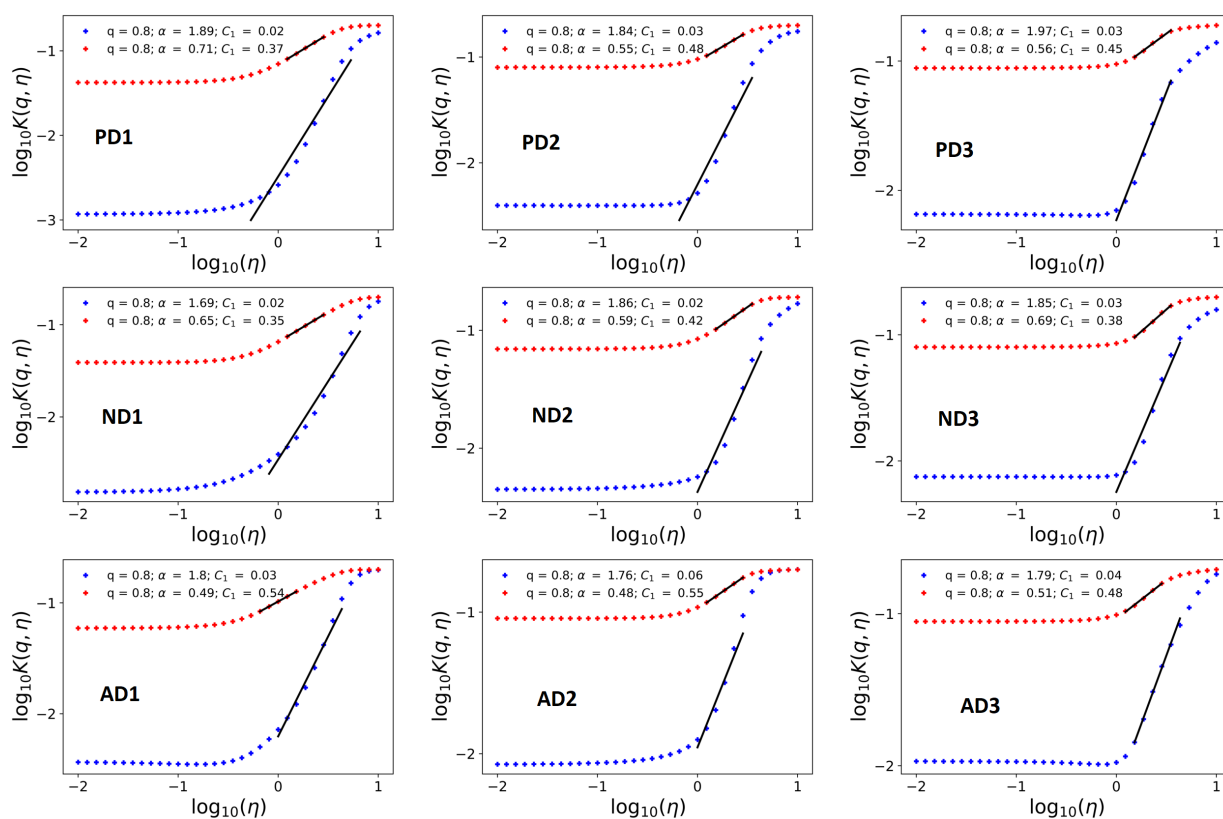


**Figure 4.** Double Trace Moment Analysis of accumulated rainfall data to obtain UM parameter estimates. Top Row: Paris: PD1, PD2, PD3; Middle Row: Nantes: ND1, ND2, ND3, and Bottom Row: Aix: AD1, AD2, AD3. The first scaling regime is shown in blue whereas the second scaling regime is shown in red.

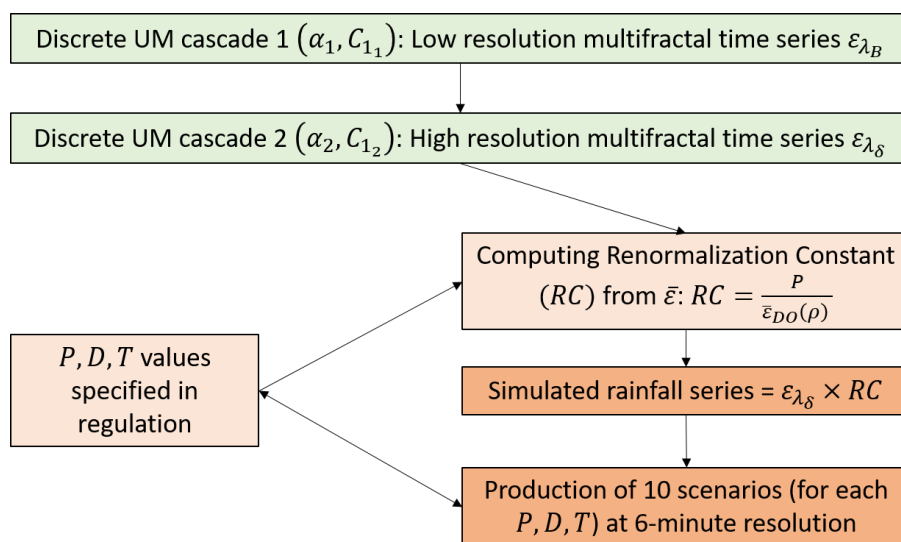


**Figure 5.** Schematic illustration of the simulation procedure used in this study to generate reference rainfall scenarios.

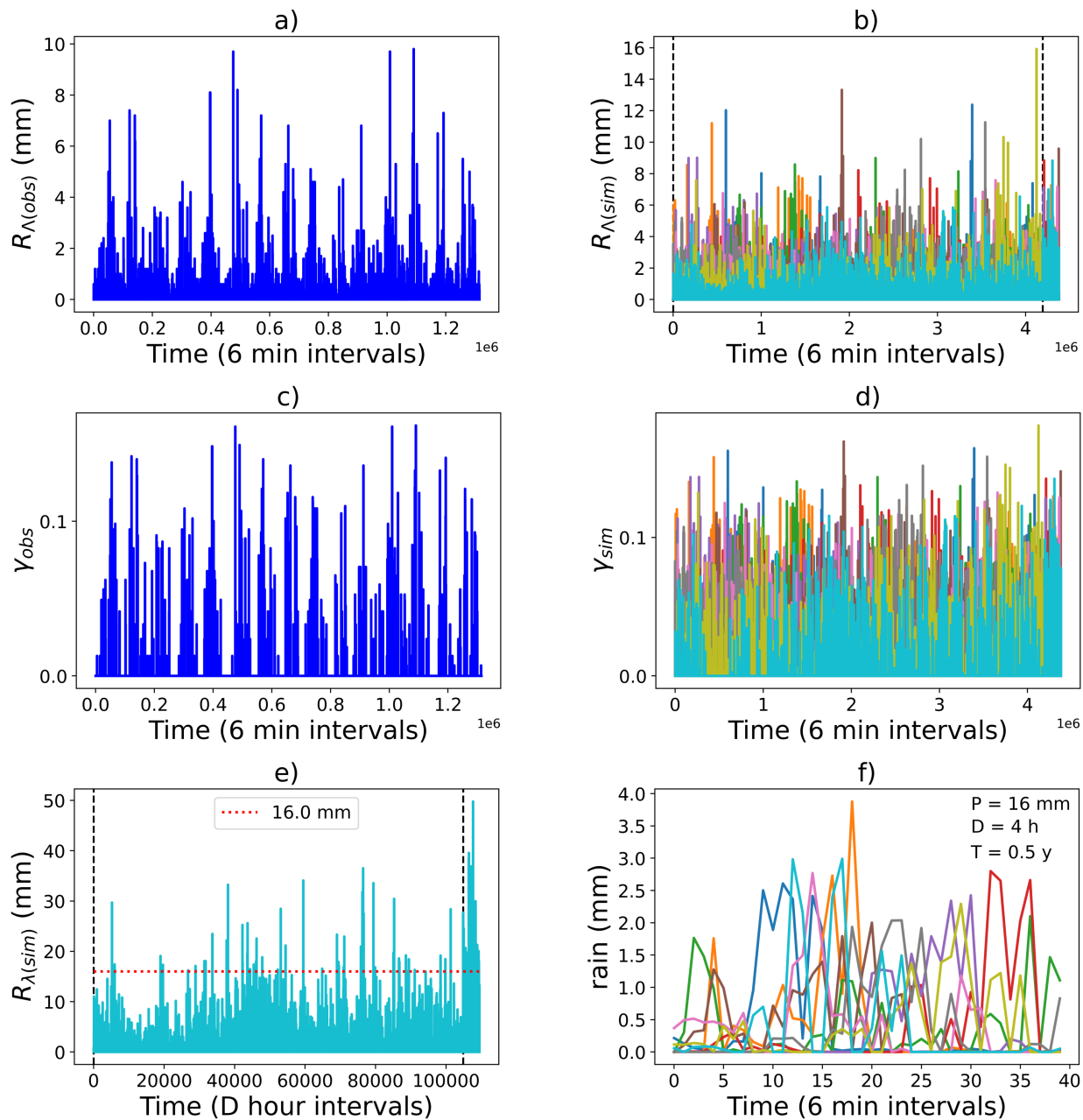


**Figure 6.** Paris reference rainfall scenarios ( $P = 16$  mm,  $D = 4$  hours,  $T = 0.5$  years). a) Rainfall and c) corresponding singularities from observational dataset PD3; b) Rainfall, d) corresponding singularities, e) aggregated rainfall from member m10 and f) events with 16 mm cumulative rainfall in 4 hours duration from the ensemble double cascade simulation.

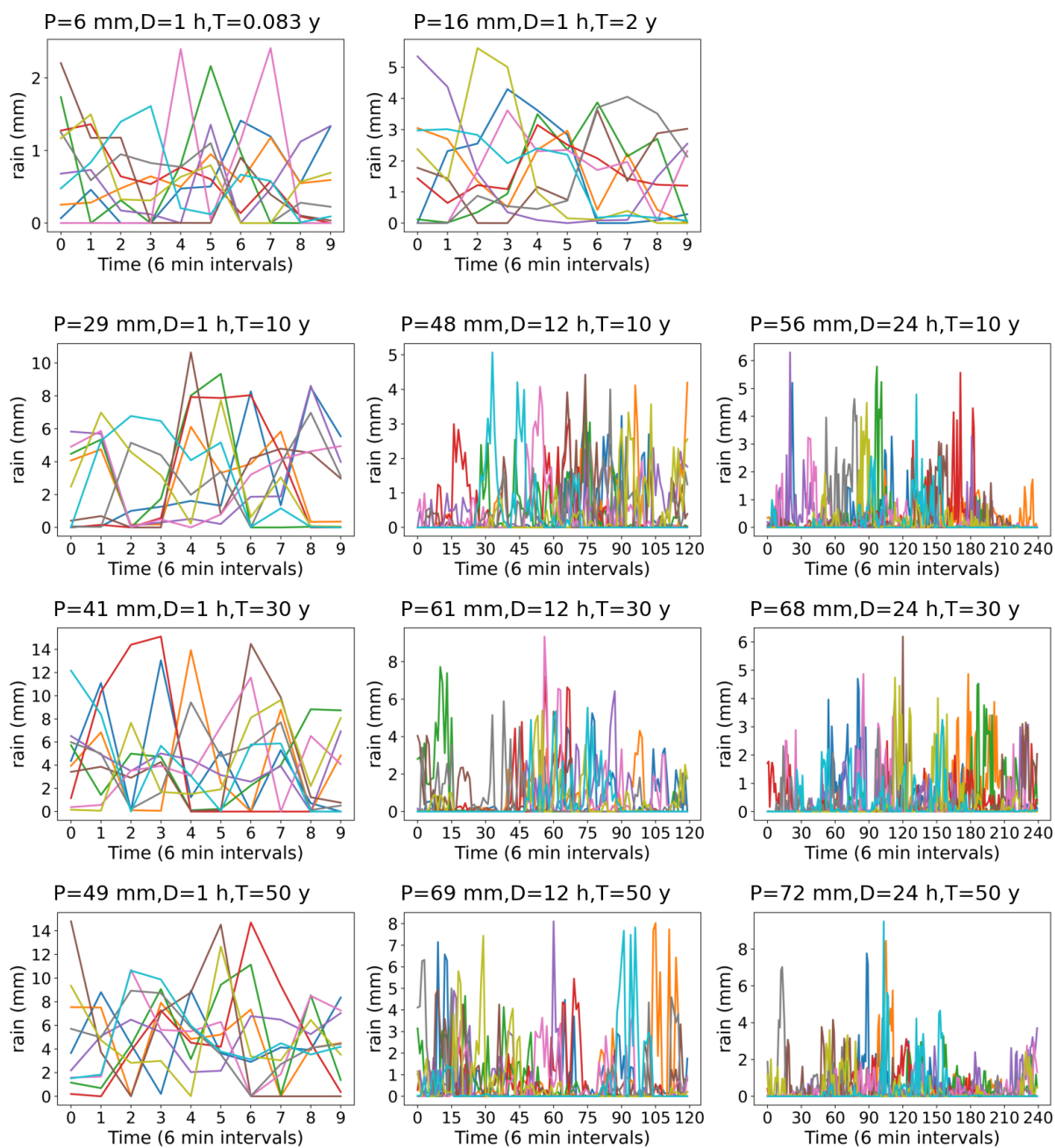


**Figure 7.** Ten rainfall scenarios (indicated by different colours) for Nantes with  $P$  mm rainfall in  $D$  hours (events such as these or more severe than these occur with a return period of  $T$  years).

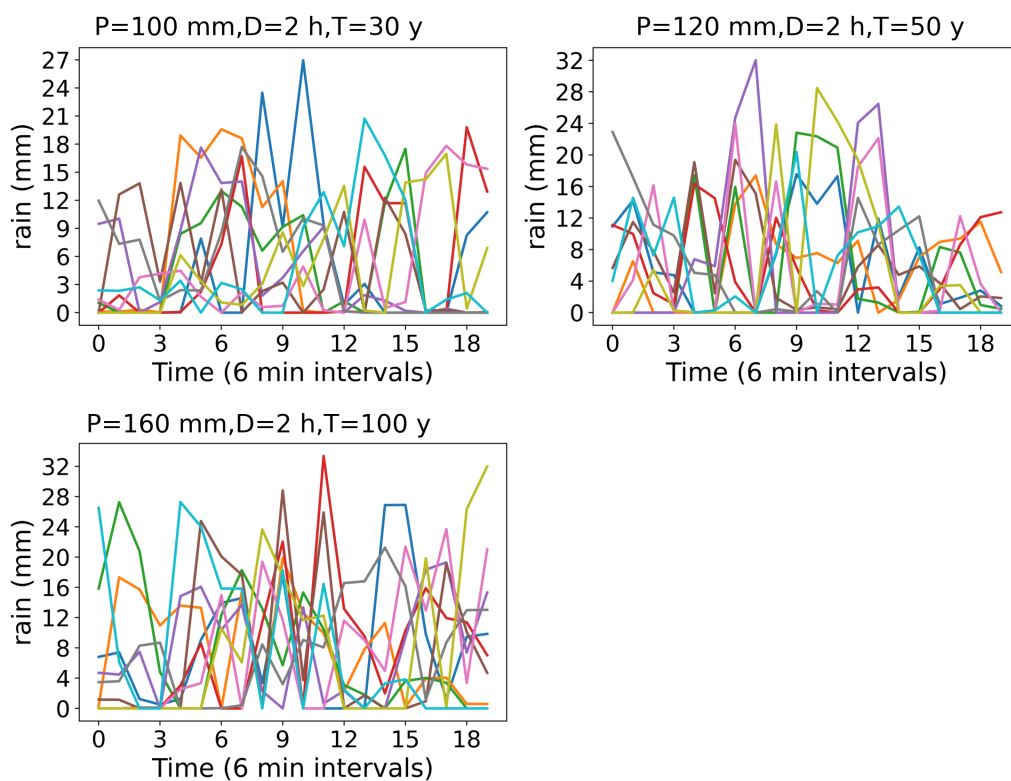


**Figure 8.** Ten rainfall scenarios (indicated by different colours) for Aix-en-Provence with  $P$  mm rainfall in  $D$  hours (events such as these or more severe than these occur with a return period of  $T$  years).

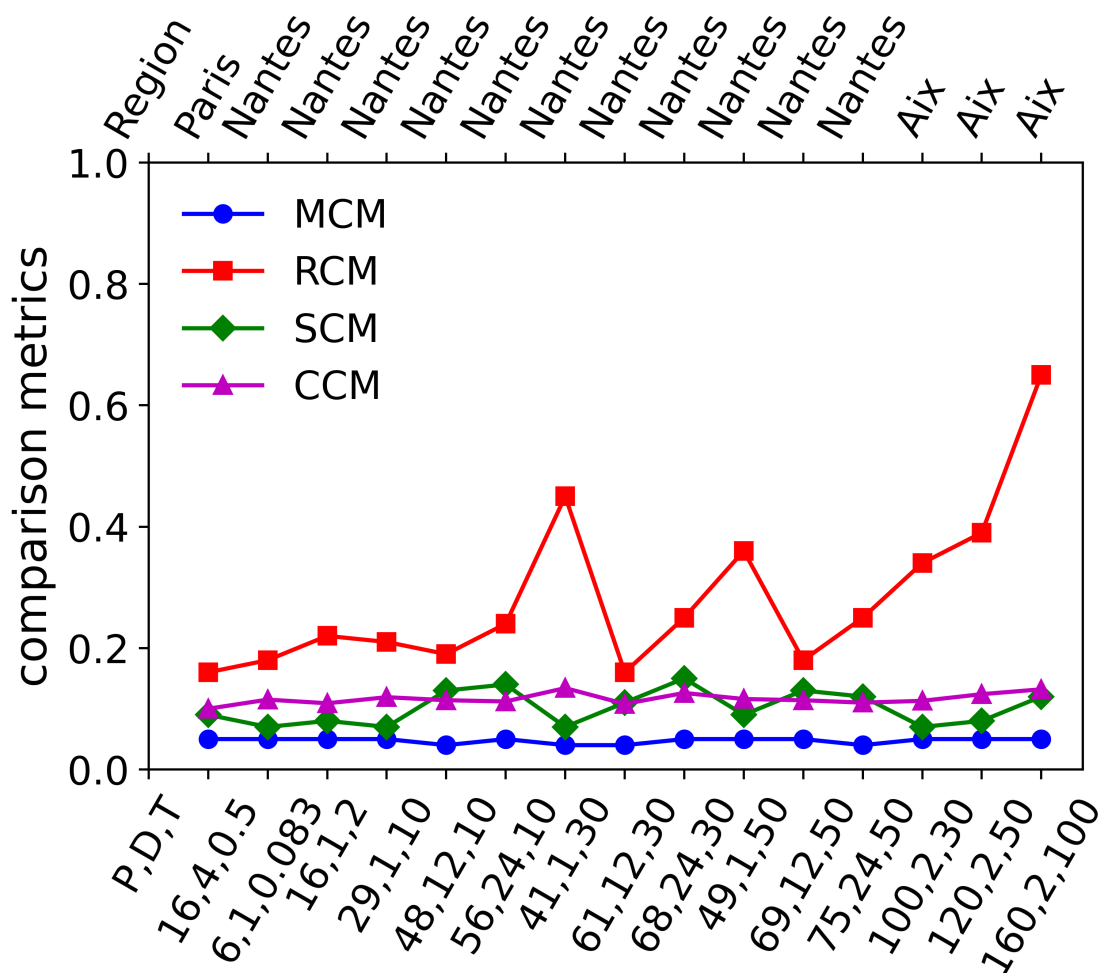


**Figure 9.** Multifractal Comparison Metric, Rainfall Comparison Metric, Singularity Comparison Metric and Codimension Comparison Metric for all the different reference rainfall simulations.  $P,D,T$  are in units of mm, hours and years respectively.